Fabrication of fluoride nanocrystals and their spectroscopic properties

N. PAWLIK[1*], B. SZPIKOWSKA-SROKA[1], T. GORYCZKA[2], W.A. PISARSKI[1]

[1]University of Silesia, Institute of Chemistry,
 Szkolna 9 Street, 40-007 Katowice, Poland

[2]Univeristy of Silesia, Institute of Materials Science,
 75 Pułku Piechoty 1A Street, 41-500 Chorzów, Poland

*Corresponding author: natalia.pawlik@smcebi.edu.pl

In this work, the fabrication of glass-ceramic materials containing MF_3:Eu^{3+} (M = La, Gd) nanocrystals dispersed in silica sol-gel hosts has been presented. The transformation from liquid sols towards bulk samples was also examined based on IR measurements. The crystallization temperatures and formation of MF_3 phases were verified based on TG/DSC analysis and XRD measurements. The optical properties of prepared Eu^{3+}-doped samples were evaluated based on PLE and PL as well as luminescence decay analysis of the $^5D_0$ excited state. Obtained samples exhibit a series of the $^5D_0 \rightarrow {}^7F_J$ (J = 1–4) emission bands, which were recorded within the reddish-orange spectral area under near-UV illumination (λ_{exc} = 393 nm). Recorded luminescence spectra and double-exponential character of decay curves for prepared glass-ceramic samples indicated the successful migration of Eu^{3+} dopant ions from amorphous silica framework to low-phonon energy MF_3 nanocrystal phases.

Keywords: sol-gel method, glass-ceramics, fluoride nanocrystals, europium ions.

1. Introduction

Nowadays, the sol-gel technique has found a very extensive application for the design and synthesis of various kinds of advanced functional and engineering materials, including powders, films, fibers, monoliths, nanostructures and organic-inorganic hybrids [1, 2]. The advantages of sol-gel method include high purity, possibility to forming many shapes, atomic-scale mixing, large compositional flexibility, and low-temperature viscous-sintering [3]. The sol-gel process involves the synthesis of three-dimensional network by a chemical reaction in a solution at low temperatures followed by the transition from liquid to colloidal sol and finally, to a solid from [1]. The factors that primarily affect the resulting structure of sol-gel materials are: pH value of hydrolyzed solution [4, 5], type of used solvent [6, 7] as well as hydrolysis and

condensation time [8, 9]. Heat treatment conditions are also important in sol-gel processing due to the possibility of removing the surface hydroxyl groups and densifying the structure to produce a ceramic monoliths or crystalline materials [10–12].

In general, fluorides are highly efficient hosts for Ln^{3+} ions due to restricted electron-phonon coupling responsible for low probability of non-radiative quenching of excited states via multiphonon relaxation [13]. Furthermore, fluorides are considered as biocompatible, nontoxic and chemically stable media, what favors a wide range of their applications [14–17]. It was pointed out that the polytypes of LnF_3 (hexagonal or orthorhombic) depentent on ionic radius and coordination number of the lanthanide ion. When the ionic radius of the lanthanide ion increases, the repulsive energy between fluoride ions decreases, what stabilizes the hexagonal phase. A critical ratio of R_{Ln}/R_F (R_{Ln} – radius of lanthanide ion, R_F – radius of fluoride ion) has been proposed to be 0.94. Therefore, it is well known that lanthanide fluorides from La^{3+} to Pm^{3+} crystallize in hexagonal phase and from Gd3+ to Lu3+ in orthorhombic modification. The critical radius ratio is positioned between Sm^{3+} and Eu^{3+}. Hence, SmF_3 and EuF_3 are known to exist in both orthorhombic and hexagonal polytypes [19].

The trivalent europium ions are frequently used as spectroscopic probes due to the characteristic nature of their electronic transitions from the $^5D_0$ excited state to the ground ^7F_J levels. Among them, the $^5D_0 \rightarrow {}^7F_1$ transition has a magnetic-dipole (MD) character, which is allowed by the Laporte selection rule and its intensity is rather independent of the local environment. In many fluoride-containing compounds or materials, the $^5D_0 \rightarrow {}^7F_1$ transition is recorded as the most intense luminescence line. On the contrary, the $^5D_0 \rightarrow {}^7F_2$ transition has an electric-dipole (ED) nature and it is so-called as hypersensitive transition. It means that its intensity is much more influenced by the local symmetry of the Eu^{3+} ion compared with the intensities of other ED transitions. Therefore, the intensities of the $^5D_0 \rightarrow {}^7F_2$ ED hypersensitive transition as well as the $^5D_0 \rightarrow {}^7F_1$ MD one are often used as a measure for the local asymmetry around Eu^{3+} in the surrounding framework [20–22].

2. Experiment

The silica xerogels doped with Eu^{3+} ions with the nominal molar ratio (in mol%) were prepared:

i) 6.3TEOS–25.1C_2H_5OH–62.7H_2O–3.14CH_3COOH–2.28TFA–0.46La(CH_3COO)$_3$–0.02Eu(CH_3COO)$_3$ (SG1), and

ii) 6.3TEOS–25.1C_2H_5OH–62.7H_2O–3.14CH_3COOH–2.28TFA–0.46Gd(CH_3COO)$_3$–0.02Eu(CH_3COO)$_3$ (SG2).

In presented procedure, each mixture of TEOS, ethyl alcohol, water and acetic acid was stirred for 30 minutes. Simultaneously, lanthanum(III) or gadolinium(III) and europium(III) acetates were dissolved in TFA acid and water, and introduced into prepared TEOS-based mixtures. Such solutions were vigorously mixed for another 60 minutes and resultant wet-gels were dried at 35°C for 7 weeks to form silica transparent xerogels. Finally, the precursor xerogels were annealed in a muffle furnace (FCF 5 5SHP produced

by Czylok, Poland) at 350°C to form glass-ceramic materials (SG1 HT and SG2 HT). The temperature was raised by 10°C/min until direct temperature was achieved. The samples were annealed for 10 hours. After this time, resulted glass-ceramic materials were cooled down to room temperature in a closed furnace.

The samples were characterized by a SETARAM Labsys thermal analyzer using the TG and DSC method. The curves were acquired with heating rate of 10°C/min. To verify the nature of prepared samples and to identify the crystal phase, the XRD analysis was carried out using X'Pert Pro diffractometer with Cu Kα radiation. In order to examine the structural properties of prepared silica sol-gel samples, the IR-ATR spectra were performed on the Nicolet iS50 ATR spectrometer. The luminescence measurements were performed using a HORIBA Jobin Yvon FluoroMax-4 spectrofluorimeter with 150 W xenon lamp as a light source. The spectral resolution was ±0.1 nm. The decay curves were detected with the accuracy of ±2 μs. The synthesis as well as photoluminescence measurements were carried out at room temperature.

3. Results and discussion

3.1. Structural and thermal characterization of fabricated sol-gel samples

The infrared spectra registered for fabricated samples at subsequent stages of presented sol-gel synthesis were presented in Fig. 1. The assignment of recorded IR signals was performed based on following papers [23, 24]. The liquid sols (Fig. 1, spectra *a–d*) are particularly rich in water and organic solvents, which were used during presented sol-gel synthesis. It was evidenced by strong OH-band at high-frequency region above 3000 cm^{-1} and signals coming from C–H vibrations located at 2975, 2926, 2898, 1450, 1395 and 1279 cm^{-1}. The signals originated from acetic acid used as a catalyst were also detected at 1719, 1651 and 882 cm^{-1} frequency regions of recorded IR spectra. It is worth noting that the impressive amounts of hydrogen-bonded Si–OH moieties (signal near ~3380 cm^{-1}) were formed even in starting solution, what proves the immediate hydrolysis reaction of TEOS after mixing the starting chemical components.

The next steps of sol-gel transformation are closely related with gradual evaporation of organic compounds and water molecules from dynamic microporous silicate structures (Fig. 1, spectra *e–k*). Indeed, the broad OH-band located at high-vibrational frequency region began to decrease, similarly as in the case of C–H signals mainly coming from volatile organic compounds, which were successfully eliminated from created silica pores. The C–H signals from organic molecules were quite-visible even after 1 week from sol-gel synthesis (Fig. 1, spectrum *e*). We suppose that such phenomenon could be explained by successfully "trapping" of such organic solvents inside a microporous silicate network due to a strong hydrogen-bonding with unreacted Si–OH groups. It was also observed that the polycondensation reaction was started at early stages of sol-gel evolution – particularly during *liquid sol* (Fig. 1, spectra *a–d*) → *wet gel* (Fig. 1, spectrum *e*) transformation – due to the IR signals originated from Si–O–Si siloxane bridges (1203 and 802 cm^{-1}), SiO$_4$ silica tetrahedrons within Q^4 units (1145 cm^{-1}), Q^3 units (1048 cm^{-1}) as well as Q^2 units (953 cm^{-1}). It was also observed that the
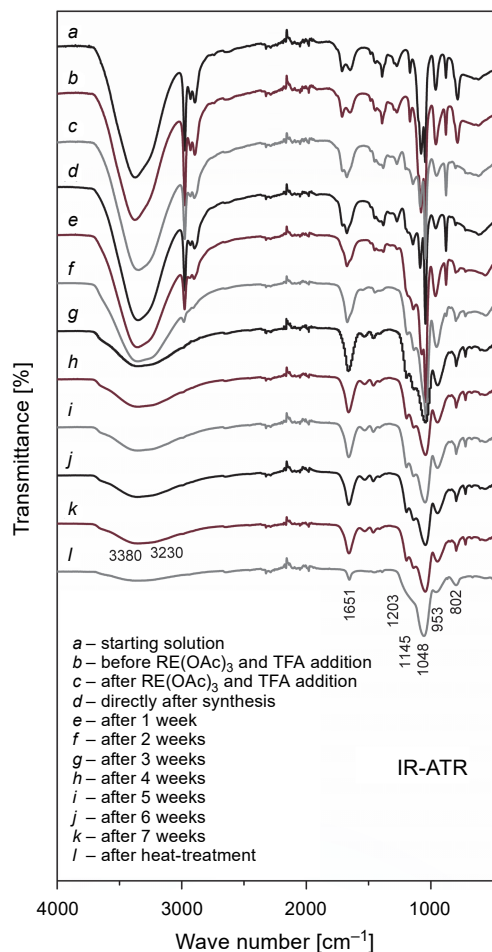
Fig. 1. IR-ATR spectra registered for fabricated samples at subsequent stages of sol-gel synthesis and after preparation; $RE(OAc)_3 = RE(CH_3COO)_3$, RE = La/Gd, Eu.

amounts of hydrogen-bonded Si–OH groups (3380 cm^{-1}) drastically decreased, what confirms that the cross-linked network was still successfully created during polycondensation reaction. Furthermore, it should be noted, that the infrared peaks located at 1203 and 1145 cm^{-1} are also assigned to C–F vibrations within trifluoroacetates. Indeed, the indicated bands appear immediately after the introduction of acetates and TFA to TEOS-based mixtures (Fig. 1, spectrum *c*). During the next time intervals, the indicated peaks develop more and more intensively, what may suggests the further creation of Si–O–Si bridges and Q^4 units. We can also conclude that further Q^n units transformations should be taken into consideration, what points that polycondensation was still in progress during *liquid sols* (Fig. 1, spectra *a–d*) → *xerogels* (Fig. 1, spectra *e–k*) evolution. Generally, the IR peak related with vibrations within SiO_4 tetrahedrons from

Q^3 units (~1048 cm^{-1}) clearly decreased what may prove the transformation towards $Q^3 \rightarrow Q^4$ units. Indeed, similar behavior was observed for 953 cm^{-1} signal (SiO$_4$ tetrahedrons inside Q^2 units), related with the $Q^2 \rightarrow Q^n$ (n = 3, 4) transformation. It was also observed that the intensity of infrared signal located near 1670 cm^{-1} region grow directly after introducing the La(III) or Gd(III) and Eu(III) salts dissolved in TFA acid (vibrations of C=O groups) (Fig. 1, spectrum c). Such IR band is also related with Si–OH vibrations. Initially, the intensity of this band decreases, which is associated with the evaporation of acetic acid and TFA residues, as well as the transformation of Si–OH groups into Si–O–Si bridges. However, the intensity of this band begins to slightly increase, which may be related with the densification effect of prepared sol-gel materials. The formation of non-hydrogen-bonded Si–OH groups was also confirmed due to the appearance of a weak band at 3660 cm^{-1} after 3 weeks from synthesis (Fig. 1, spectrum g). Such non-hydrogen-bonded Si–OH groups confirmed the progressive enhancement of polycondensation reaction and dynamic character of obtained wet-gels. Such dynamic character of prepared gels could be also confirmed by a growing number of Si–O–Si siloxane bridges formed within silica network (~802 cm^{-1}).

To evaluate the thermal resistance of precursor xerogels and to identify the transition temperatures, the TG/DSC analysis was carried out in a temperature range from 50 up to 500°C (Fig. 2). The crystallization of MF$_3$ (M = La, Gd) nanophases is associated with thermal degradation of appropriate trifluoroacetate, *i.e.* La(CF$_3$COO)$_3$ or Gd(CF$_3$COO)$_3$ and the crystallization temperatures were identified based on DSC exothermic peaks with maxima at 307 and 313°C, respectively. The formation of MF$_3$ nanocrystals is realized via a homogeneous nucleation through a controlled fluorination of the M–O bond into the M–F one by using F$^-$ ions coming from the cleavage of the C–F bond from trifluoroacetate ligands during thermolysis [25]. It was observed that the thermal degradation of La(CF$_3$COO)$_3$ is a bit more effective (22.17% weight loss) compared to Gd(CF$_3$COO)$_3$ (18.89% weight loss). Furthermore, based on presented
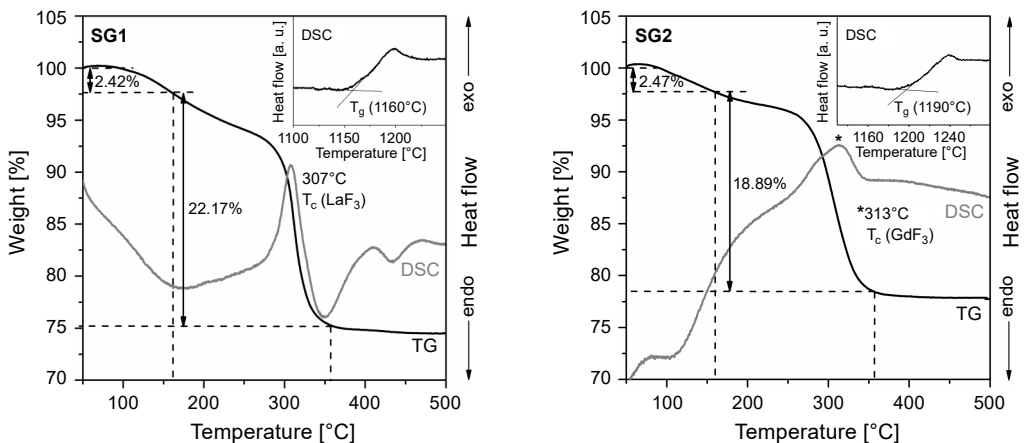

Fig. 2. TG/DSC curves for prepared silica xerogels.

TG results, the resultant silica sol-gel hosts are almost completely thermally stable at 350°C, therefore, such temperature was chosen to carry out the controlled ceramization process to precipitate the LaF_3:Eu^{3+} and GdF_3:Eu^{3+} crystal phases dispersed within silica hosts.

Moreover, the glass transition temperatures T_g were also evaluated for studied sol-gel samples, which were identified at 1160 and 1190°C for SG1 and SG2, respectively. It is quite interesting, because the crystallization temperatures of LaF_3 and GdF_3 are much lower than T_g of fabricated samples. In contrary to sol-gel materials, the oxyfluoride glasses prepared by the melt-quenching technique are treated at temperatures slightly higher than T_g to fabrication the fluoride crystals [26]. The detailed discussion in a field of crystallization in oxyfluoride sol-gel materials were performed in excellent research paper by Gorni *et al*. [27]. The authors stated that crystallization in sol-gel materials is not a diffusion-controlled process – as for melt-quenched glasses – but a chemical reaction followed by a fast precipitation of fluoride crystals. This property of oxyfluoride sol-gel materials allows for successful fabrication of fluoride nanocrystals dispersed within the oxide matrix at relatively low temperatures.

To verify the nature of fabricated sol-gel samples, the X-ray diffraction (XRD) measurements were performed and the results were depicted in Fig. 3. The halo patterns *e*
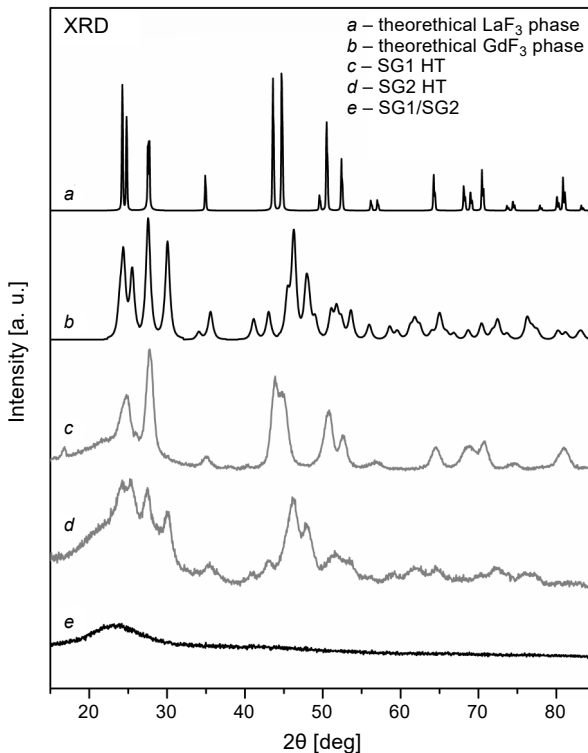

Fig. 3. X-ray diffraction patterns for Eu^{3+}-doped sol-gel samples before and after annealing at 350°C per 10 hours.

clearly identified the amorphous nature of precursor sol-gel samples before the performed ceramization process. Compared with standard patterns of hexagonal LaF_3 phase as well as orthorhombic GdF_3 phase (*a* and *b*), the results of XRD measurements indicated that LaF_3 and GdF_3 crystals were well crystallized (*c* and *d*). The broadening of recorded diffraction lines obviously indicates that formed MF_3 crystals are in a nanometric range. The MF_3 crystal sizes were estimated using the Scherrer equation and the mean values were equaled to 8.1 nm for LaF_3 and 6.3 nm for GdF_3. Some shift of diffraction lines has been observed for both types of prepared samples compared with standard patterns for LaF_3 and GdF_3 phases. Indeed, if Eu^{3+} substitutes La^{3+} or Gd^{3+} ions within MF_3 (M = La, Gd) crystal lattices, the cell volume will be changed to a certain extent inducing a peak shifting of XRD diffraction lines. Therefore, such slight shift of diffraction lines was observed, what could be a proof for entering of Eu^{3+} ions into precipitated LaF_3 and GdF_3 crystal lattices. The indicated effect is better visible for SG1 HT glass-ceramic samples with dispersed LaF_3 nanocrystal phase due to a larger difference in ionic radii between Eu^{3+} (1.07 Å) and La^{3+} (1.16 Å), compared to Gd^{3+} (1.05 Å).

Based on performed IR (Fig. 1, spectrum *l*) as well as XRD (Fig. 3) measurements, it was found that applied annealing conditions of xerogels (350°C per 10 hours) allow for successful crystallization of LaF_3 and GdF_3 phases in a nanometric range as well as for an effective removal of water and organic compounds from the porous silicate network.

3.2. Optical characterization of prepared Eu^{3+}-doped sol-gel materials

Figure 4 presents the PLE excitation spectra as well as PL emission spectra for fabricated sol-gel samples. The PLE spectra were recorded from 340 to 475 nm spectral range and monitored at λ_{em} = 611 nm emission line (the $^5D_0 \rightarrow {}^7F_2$ transition of Eu^{3+}). Registered narrow excitation bands are related to the typical $4f^6$–$4f^6$ intra-configurational
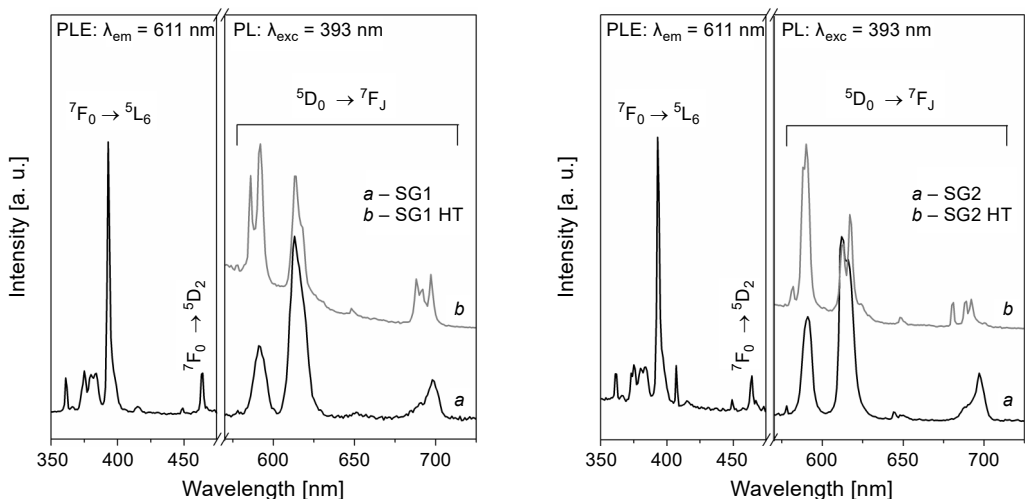

Fig. 4. PLE and PL spectra registered for studied sol-gel materials.

electronic transitions of Eu^{3+}, which can be assigned to populating the upper-lying $^5L_6$ and $^5D_2$ levels from the $^7F_0$ ground state. The most prominent line corresponds to the $^7F_0 \rightarrow {}^5L_6$ transition with maximum located at $\lambda_{exc} = 393$ nm.

Recorded PL spectra consist of the characteristic intra-configurational luminescence lines related with electronic transitions from the $^5D_0$ excited state to the ^7F_J ground levels. The four characteristic emission bands of Eu^{3+} ions were observed within the reddish-orange light area at: $\lambda_{em} = 590$ nm ($^5D_0 \rightarrow {}^7F_1$), $\lambda_{em} = 611$ nm ($^5D_0 \rightarrow {}^7F_2$), $\lambda_{em} = 645$ nm ($^5D_0 \rightarrow {}^7F_3$) and $\lambda_{em} = 698$ nm ($^5D_0 \rightarrow {}^7F_4$). The strong splitting of registered photoluminescence bands has been observed and the maxima were located at: 582 nm ($^5D_0 \rightarrow {}^7F_0$), 588 nm, 590 nm ($^5D_0 \rightarrow {}^7F_1$ splitted for SG1 HT)/586 nm, 592 nm ($^5D_0 \rightarrow {}^7F_1$ splitted for SG2 HT), 611 nm, 617 nm ($^5D_0 \rightarrow {}^7F_2$ splitted), 648 nm ($^5D_0 \rightarrow {}^7F_3$), 680 nm, 689 nm, 692 nm ($^5D_0 \rightarrow {}^7F_4$ splitted).

The splitting of emission bands after ceramization process is a consequence of incorporation of Eu^{3+} optically active ions into MF_3 nanocrystal lattice created during heat-treatment and the relative intensities as well as splitting of emission bands are ruled by the local symmetry. Moreover, due to the nature of the $^5D_0 \rightarrow {}^7F_J$ ($J = 1, 2$) transitions, the red-to-orange luminescence intensity ratio (R/O = $I(^5D_0 \rightarrow {}^7F_2)/I(^5D_0 \rightarrow {}^7F_1)$) can be viewed as a clue concerning the structural symmetry in which Eu^{3+} is located. For amorphous xerogels the $^5D_0 \rightarrow {}^7F_2$ red emission band has the greatest intensity, meanwhile the $^5D_0 \rightarrow {}^7F_1$ orange line is the most prominent emission peak for prepared glass-ceramic samples. The calculated values of R/O-factor for xerogels are equal to 2.37 and 3.09 for SG1 and SG2 samples, meanwhile for glass-ceramic materials, the R/O-ratio values are equal to and 0.78 and 0.89 for SG1 HT and SG2 HT. Indicated decrease in R/O-ratio values proves that there is a radical change in chemical environment around optically active Eu^{3+} ions during performed ceramization process. Such R/O-factor informs about covalence bonding between Eu^{3+} ion and its nearest surrounding, and R/O-ratio increases with increasing asymmetry and covalency. From this point of view, various R/O-factor values calculated for xerogel samples could be probably explained by differences in electronegativity of La ($\chi = 1.1$) and Gd ($\chi = 1.2$). A slightly lower R/O-ratio value was reported for SG1 HT sample compared with SG2 HT. In the hexagonal matrix of LaF_3, Eu^{3+} ion is located at a site of C_2 symmetry, where ED ($^5D_0 \rightarrow {}^7F_2$) and MD ($^5D_0 \rightarrow {}^7F_1$) transitions are both allowed. In the case of orthorhombic GdF_3 phase, Eu^{3+} ion is presented at C_s sites in which both ED and MD transitions are also allowed similarly as in the case of C_2 sites within LaF_3 hexagonal phase. However, the orthorhombic crystallographic class is a group with relatively low symmetry, similarly as in the case of monoclinic or triclinic groups. Therefore, calculated R/O-factor is lower for SG1 HT glass-ceramic samples with distributed LaF_3 nanocrystals due to higher local symmetry around Eu^{3+} dopant ions.

In order to perform the further photoluminescence characterization of prepared Eu^{3+}-doped sol-gel samples, the decay curves of the $^5D_0$ excited state were also registered and analyzed (Fig. 5). The decay curves were recorded for the $\lambda_{em} = 611$ nm emission line ($^5D_0 \rightarrow {}^7F_2$ transition) using the $\lambda_{exc} = 393$ nm near-UV light ($^7F_0 \rightarrow {}^5L_6$ transition) as an excitation source. The decay curves registered for amorphous xerogel samples
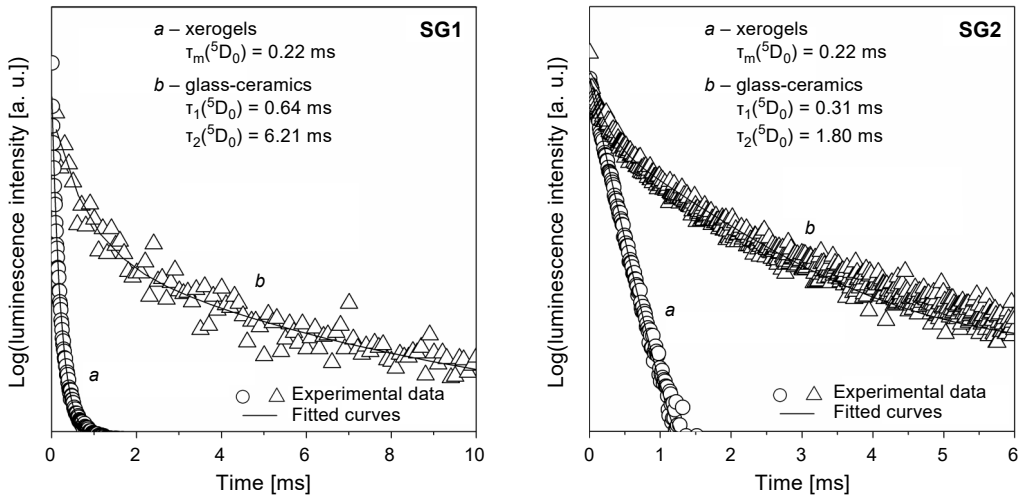
Fig. 5. Decay curves for the $^5D_0$ excited state of Eu^{3+} ions recorded under near-UV illumination.

are well-fitted to the single-exponential functions and the calculated lifetime is equaled to $\tau_m = 0.22$ ms both for SG1 and SG2 samples. Such relatively short lifetime is correlated with presence of high-vibrational OH quenching channels, which are coming from water molecules, organic residues and Si–OH groups within prepared sol-gel hosts. The energy of the $^5D_0$ excited level of Eu^{3+} is close to the $v = 4$ integer number of OH vibrational quanta [28]. Hence, the rapid non-radiative multiphonon relaxation through OH groups can occur, determining simultaneously the radiative decay rate from the $^5D_0$ level of dopant ions (Eu^{3+}).

The decay curves registered for prepared glass-ceramic samples are well-fitted to double-exponential functions. It indicates that Eu^{3+} ions are located in two different sites with different decay rates. The luminescence decay consists of rapid decay component with lifetimes equaled to $\tau_{m1} = 0.64$ ms (SG1 HT) and $\tau_{m1} = 0.31$ ms (SG2 HT) as well as slow decay element with lifetimes equaled to $\tau_{m2} = 6.21$ ms (SG1 HT) and $\tau_{m2} = 1.80$ ms (SG2 HT). The rapid decay component is related with this part of Eu^{3+} ions which are still present in high-vibrational amorphous silica network. As was proven in IR-ATR spectrum, silanol Si–OH moieties with maximum at ~3380 cm^{-1} frequency region are still present after performed heat-treatment process. In this case, indicated groups are responsible for effective quenching of the luminescence from the $^5D_0$ excited state of Eu^{3+}. We suppose that a higher value of τ_{m1} for SG1 HT than for SG2 HT samples could be associated with the presence of Eu^{3+} ions in a local symmetry closer to the inversion center (near hexagonal LaF_3 nanocrystal phase). The second lifetime component τ_{m2} is prolonged and it is related with this part of Eu^{3+} ions which are located on the surface of MF_3 nanoparticles with low-phonon energy. In this case, up to ~36 phonons of MF_3 crystal lattice are needed to cover the $^5D_0 \rightarrow {}^7F_J$ energy gap which is equal to $\Delta E = 12500$ cm^{-1} [29], and therefore, such lifetime components are prolonged. It was observed that the τ_{m2} lifetime component is more than 3-times

longer for SG1 HT samples compared with SG2 HT. Due to the comparable phonon energies of both crystal lattices, *i.e.* LaF_3 and GdF_3, which are equal to ~350 cm^{-1}, we supposed that the decisive influence on extending the luminescence lifetime for SG1 HT samples may have more efficient incorporation of Eu^{3+} ions in LaF_3 phase than in GdF_3 one. Indeed, based on presented TG curves, we can conclude that thermal degradation of $La(CF_3COO)_3$ is slightly more efficient than $Gd(CF_3COO)_3$, what promoted the formation of LaF_3 crystal fraction compared with GdF_3. Additionally, based on XRD studies, precipitated GdF_3 crystallites have smaller diameter compared with LaF_3 nanocrystals, what may also favor the retain of higher amounts of Eu^{3+} ions on the GdF_3 particles' surface, where Eu^{3+} ions still have a "contact" with the high-vibrational silica surrounding. The double-exponential character of luminescence decay curves indicated the distribution of Eu^{3+} ions between low-phonon crystal phases and amorphous silica framework.

4. Conclusions

The silica xerogels were fabricated using the mild sol-gel technique and finally they were successfully transformed during the controlled ceramization process into glass-ceramic materials with dispersed MF_3 (M = La, Gd) nanocrystalline phases. The composition of prepared xerogels allowed for such transformation at relatively low temperature (350°C) due to the thermal degradation of appropriate trifluoroacetates, *i.e.* $M(CF_3COO)_3$ (M = La, Gd). The LaF_3 and GdF_3 crystal phases were identified based on XRD measurements and the average nanocrystal sizes were estimated to 8.1 nm (LaF_3) and 6.3 nm (GdF_3) using the Scherrer equation. Additionally, the oscillation frequencies of functional groups and chemical linkages formed within prepared materials during sol-gel evolution were also evidenced using IR-ATR spectroscopy. Moreover, in order to characterize the luminescence behavior of prepared Eu^{3+}-doped samples, the PLE and PL spectra as well as luminescence decay curves were registered. The characteristic electronic transitions within $4f^6$ manifold of Eu^{3+} were recorded. The amorphous silica sol-gel samples before ceramization exhibited monoexponential decay profiles, however, for glass-ceramic materials the detected decay curves were well-fitted to biexponential functions. In accordance with calculated R/O-factor values, we can suggest that Eu^{3+} optically active ions were effectively incorporated into precipitated MF_3 (M = La, Gd) nanocrystals.

References

[1] Lin J., Yu M., Lin C., Liu X., *Multiform oxide optical materials via the versatile Pechini-type sol-gel process: synthesis and characteristics*, The Journal of Physical Chemistry C **111**(16), 2007, pp. 5835 –5845, DOI: 10.1021/jp070062c.

[2] Pénard A.L., Gacoin T., Boilot J.P., *Functionalized sol-gel coatings for optical applications*, Accounts of Chemical Research **40**(9), 2007, pp. 895–902, DOI: 10.1021/ar600025j.

[3] BALLATO J., RIMAN R.E., SNITZER E., *Sol-gel synthesis of fluoride optical materials for planar integrated photonic applications*, Journal of Non-Crystalline Solids **213-214**, 1997, pp. 126–136, DOI: 10.1016/S0022-3093(97)00053-7.

[4] CARUSO R., DE SANCTIS O., MARCÍAS-GARCÍA A., BENAVIDEZ E., MINTZER S.R., *Influence of pH value and solvent utilized in the sol-gel synthesis on properties of derived ZrO_2 powders*, Journal of Materials Processing Technology **152**(3), 2004, pp. 299–303, DOI: 10.1016/j.jmatprotec.2004.04.371.

[5] SILVA R.F., VASCONCELOS W.L., *Influence of processing variables on the pore structure of silica gels obtained with tetraethylorthosilicate*, Materials Research **2**(3), 1999, pp. 197–200, DOI: 10.1590/S1516-14391999000300014.

[6] LIU X., JIN Z., BU S., YIN T., *Influences of solvent on properties of TiO_2 porous films prepared by a sol-gel method from the system containing PEG*, Journal of Sol-Gel Science and Technology **36**(1), 2005, pp. 103–111, DOI: 10.1007/s10971-005-2746-6.

[7] GONZÁLEZ M.B., WU A., VILARINHO P.M., *Influence of solvents on the microstructure and dielectric properties of $Ba_{0.5}Sr_{0.5}TiO_3$ thin films prepared by a diol-based sol-gel process*, Chemistry of Materials **18**(7), 2006, pp. 1737–1744, DOI: 10.1021/cm048029f.

[8] DE OLIVEIRA NASSOR E.C., ÁVILA L.R., DOS SANTOS PEREIRA P.F., CIUFFI K.J., CALEFI P.S., NASSAR E.J., *Influence of the hydrolysis and condensation time on the preparation of hybrid materials*, Materials Research **14**(1), 2011, pp. 1–6, DOI: 10.1590/S1516-14392011005000003.

[9] SASANI N., AYASK H.K., ZEBARJAD S.M., KHAKI J.V., *Characterization of rod-like high-purity fluoroapatite nanopowders obtained by sol-gel method*, Journal of Ultrafine Grained and Nanostructured Materials **46**(1), 2013, pp. 31–37, DOI: 10.7508/jufgnsm.2013.01.005.

[10] DANKS A.E., HALL S.R., SCHNEPP Z., *The evolution of 'sol-gel' chemistry as a technique for materials synthesis*, Materials Horizons **3**(2), 2016, pp. 91–112, DOI: 10.1039/C5MH00260E.

[11] BAUER J., ULATOWSKA-JARŻA A., PODBIELSKA H., LECHNA-MARCZYŃSKA M., BINDIG U., MÜLLER G., BEUTHAN J., *Influence of heating temperature on structural properties of sol-gel materials*, Optica Applicata **35**(4), 2005, pp. 791–797.

[12] MOTLOUNG S.V., TSEGA M., DEJENE F.B., SWART H.C., NTWAEABORWA O.M., KOAO L.F., MOTAUNG T.E., HATO M.J., *Effect of annealing temperature on structural and optical properties of $ZnAl_2O_4$: 1.5% Pb^{2+} nanocrystals synthesized via sol-gel reaction*, Journal of Alloys and Compounds **677**, 2016, pp. 72–79, DOI: 10.1016/j.jallcom.2016.03.170.

[13] BANSKI M., NOCULAK A., MISIEWICZ J., PODHORODECKI A., *Rice oil as a green source of capping ligands for GdF_3 nanocrystals*, New Journal of Chemistry **40**(9), 2016, pp. 7928–7934, DOI: 10.1039/C6NJ01052K.

[14] ZHANG Z.J., YANG W., *Luminescence characteristic of RE (RE = Pr, Sm, Eu, Tb, Dy) and energy levels of lanthanide ions in $Gd_5Si_3O_{12}N$*, Solid State Sciences **72**, 2017, pp. 64–70, DOI: 10.1016/j.solidstatesciences.2017.08.015.

[15] CHEN D., WANG Y., YU Y., HUANG P., *Structure and optical spectroscopy of Eu-doped glass ceramics containing GdF_3 nanocrystals*, The Journal of Physical Chemistry C **112**(48), 2008, pp. 18943–18947, DOI: 10.1021/jp808061x.

[16] LI H., LIU G., WANG J., DONG X., YU W., *Eu^{3+}/Tb^{3+} doped cubic $BaGdF_5$ multifunctional nanophosphors: multicolor tunable luminescence, energy transfer and magnetic properties*, Journal of Luminescence **186**, 2017, pp. 6–15, DOI: 10.1016/j.jlumin.2017.02.005.

[17] CAO C., GUO S., MOON B.K., CHOI B.C., JEONG J.H., *Synthesis, modified optical properties, and energy transfer of Tb^{3+} doped GdF_3*, Optics Communications **301-302**, 2013, pp. 106–111, DOI: 10.1016/j.optcom.2013.03.049.

[18] ZHANG X., HAYAKAWA T., NOGAMI M., ISHIKAWA Y., *Selective synthesis and luminescence properties of nanocrystalline GdF_3:Eu^{3+} with hexagonal and orthorhombic structures*, Journal of Nanomaterials, 2010, article ID 651326, DOI: 10.1155/2010/651326.

[19] SAYED F.N., GROVER V., SUDARSAN V., PANDEY B.N., ASTHANA A., VATSA R.K., TYAGI A.K., *Multicolored and white-light phosphors based on doped GdF_3 nanoparticles and their potential bio-applications*, Journal of Colloid and Interface Science **367**(1), 2012, pp. 161–170, DOI: 10.1016/j.jcis.2011.09.083.

[20] BINNEMANS K., *Interpretation of europium(III) spectra*, Coordination Chemistry Reviews **295**, 2015, pp. 1–45, DOI: 10.1016/j.ccr.2015.02.015.

[21] LAKSHMINARAYANA G., QIU J., BRIK M.G., KITYK I.V., *Photoluminescence of Eu^{3+}-, Tb^{3+}-, Dy^{3+}- and Tm^{3+}-doped transparent GeO_2–TiO_2–K_2O glass ceramics*, Journal of Physics: Condensed Matter **20**(33), 2008, article ID 335106, DOI: 10.1088/0953-8984/20/33/335106.

[22] LAVÍN V., RODRÍGUEZ-MENDOZA U.R., MARTÍN I.R., RODRÍGUEZ V.D., *Optical spectroscopy analysis of the Eu^{3+} ions local structure in calcium diborate glasses*, Journal of Non-Crystalline Solids **319**(1–2), 2003, pp. 200–216, DOI: 10.1016/S0022-3093(02)01914-2.

[23] SZPIKOWSKA-SROKA B., PAWLIK N., GORYCZKA T., PIETRASIK E., BAŃCZYK M., PISARSKI W.A., *Lead fluoride β-PbF_2 nanocrystals containing Eu^{3+} and Tb^{3+} ions embedded in sol-gel materials: thermal, structural and optical investigations*, Ceramics International **43**(11), 2017, pp. 8424–8432, DOI: 10.1016/j.ceramint.2017.03.192.

[24] ATKINSON I., ANGHEL E.M., PREDOANA L., MOCIOIU O.C., JECU L., RAUT I., MUNTEANU C., CULITA D., ZAHARESCU M., *Influence of ZnO addition on the structural, in vitro behavior and antimicrobial activity of sol-gel derived CaO–P_2O_5–SiO_2 bioactive glasses*, Ceramics International **42**(2), 2016, pp. 3033 –3045, DOI: 10.1016/j.ceramint.2015.10.090.

[25] YANES A.C., DEL-CASTILLO J., MÉNDEZ-RAMOS J., RODRIGUEZ V.D., TORRES M.E., ARBIOL J., *Luminescence and structural characterization of transparent nanostructures Eu^{3+}-doped LaF_3-SiO_2 glass-ceramics prepared by sol-gel method*, Optical Materials **29**(8), 2007, pp. 999–1003, DOI: 10.1016/j.optmat.2006.02.021.

[26] PISARSKA J., SOŁTYS M., JANEK J., GÓRNY A., PIETRASIK E., GORYCZKA T., PISARSKI W.A., *Crystallization of lead-based and lead-free oxyfluoride germanate glasses doped with erbium during heat treatment process*, Journal of Non-Crystalline Solids **501**, 2018, pp. 121–125, DOI: 10.1016/j.jnoncrysol.2018.01.005.

[27] GORNI G., PASCUAL M.J., CABALLERO A., VELÁZQUEZ J.J., MOSA J., CASTRO Y., DURÁN A., *Crystallization mechanism in sol-gel oxyfluoride glass-ceramics*, Journal of Non-Crystalline Solids **501**, 2018, pp. 145–152, DOI: 10.1016/j.jnoncrysol.2018.01.031.

[28] SENTY T.R., YALAMANCHI M., ZHANG Y., CUSHING S.K., SEEHRA M.S, SHI X., BRISTOW A.D., *Photoluminescence spectroscopy of YVO_4:Eu^{3+} nanoparticles with aromatic linker molecules: a precursor to biomedical functionalization*, Journal of Applied Physics **115**(16), 2014, article ID 163107, DOI: 10.1063/1.4874179.

[29] SOŁTYS M., JANEK J., ŻUR L., PISARSKA J., PISARSKI W.A., *Compositional-dependent europium-doped lead phosphate glasses and their spectroscopic properties*, Optical Materials **40**, 2015, pp. 91–96, DOI: 10.1016/j.optmat.2014.11.052.